IAEA
International Atomic Energy Agency

20th IAEA Fusion Energy Conference
Vilamoura, Portugal, 1-6 November 2004

IAEA-CN-116/EX/2-1

Energy loss for grassy ELMs and effect of plasma rotation on the ELM characteristics in JT-60U

N. Oyama 1), Y. Sakamoto 1), M. Takechi 1), A. Isayama 1), P. Gohil 2), L. L. Lao 2), P. B. Snyder 2), T. Suzuki 1), Y. Kamada 1), T. Oikawa 1), H. Takenaga 1), T. Fujita 1), S. Ide 1), Y. Miura 1), K. Toi 3), and the JT-60 Team

1) Japan Atomic Energy Research Institute,
801-1 Naka-machi, Naka-gun 311-0193, Japan

2) General Atomics, San Diego, CA 92186-5608, USA

3) National Institute for Fusion Science,
322-6 Oroshi-cho, Toki 509-5292, Japan

Energy loss for grassy ELMs and effects of plasma rotation on the ELM characteristics in JT-60U

N. Oyama 1), Y. Sakamoto 1), M. Takechi 1), A. Isayama 1), P. Gohil 2), L. L. Lao 2), P. B. Snyder 2), T. Suzuki 1), Y. Kamada 1), T. Oikawa 1), H. Takenaga 1), T. Fujita 1), S. Ide 1), Y. Miura 1), K. Toi 3), the JT-60 Team

1) Japan Atomic Energy Research Institute, 801-1 Naka-machi, Naka-gun 311-0193, Japan
2) General Atomics, San Diego, CA 92186-5608, USA
3) National Institute for Fusion Science, 322-6 Oroshi-cho, Toki 509-5292, Japan

e-mail contact of main author: oyaman@fusion.naka.jaeri.go.jp

Abstract. The energy loss for the grassy ELM has been studied to investigate the applicability of the grassy ELM regime to ITER. The grassy ELM is characterized by the high frequency periodic collapse up to ~kHz, which is ~15 times faster than that for type I ELM. A divertor peak heat flux due to grassy ELMs is less than 10% of that for type I ELMs. This smaller heat flux is caused by narrower radial extent of the collapse of temperature pedestal. The different radial extent between type I ELMs and grassy ELMs qualitatively agrees with the different radial distribution of the eigen function of the ideal MHD stability analysis. The dominant ELM energy loss for grassy ELMs seems to be conductive loss, and its ratio to the pedestal stored energy was 0.4-1%, which is smaller by factor of about 10 than that for type I ELMs of 2-10%. A good capability to change the plasma rotation actively using a combination of the tangential and perpendicular NBIs in JT-60U has clarified the effects of the counter (CTR) plasma rotation on the ELM characteristics, systematically. In high δ regime, ELM amplitude, frequency and type can be changed from type I ELM to high frequency grassy ELM as CTR plasma rotation was increased. In low δ regime, on the other hand, the complete ELM suppression (QH-mode) has been achieved, when the plasma position is optimized with CTR-NBIs. The existence of the edge fluctuations localized in pedestal region may reduce the pedestal pressure, and therefore the QH-mode can be sustained for long time up to 3.4s (~18 τ_E). In JT-60U, a transient QH phase was observed during the CO-NB injection phase with almost no edge toroidal rotation.

1. Introduction

Since the ELMy H-mode plasma is considered as a standard operation scenario in ITER, the establishment of the H-mode plasma with a small ELM is an important subject to extend the lifetime of the divertor target plate in ITER [1]. In JT-60U, an attractive operational mode in a low collisionality region (ν^*_{ped}<0.15), such as the grassy ELM regime, has been found in high safety factor (q) and high triangularity (δ) plasma [2]. Recently, we have successfully expand the operational regime of grassy ELM toward lower q region, q_{95}<4, by using higher δ plasma up to δ~0.6 [3], as shown in Fig. 1. Another alternative operational mode with tolerable divertor heat load under the low collisionality region is the quiescent H-mode (QH-mode), where similar confinement level to usual H-mode can be sustained without any ELMs. The QH-mode has been discovered in DIII-D [4], and also found in JT-60U [5] and ASDEX Upgrade [6]. In these observations, the CTR-NBI (neutral beam injection opposite to the plasma current), and a larger clearance between separatrix and first wall (especially low-field side) are required to obtain the QH phase. In this paper, we report the energy loss for grassy ELMs including ELM frequency dependence,

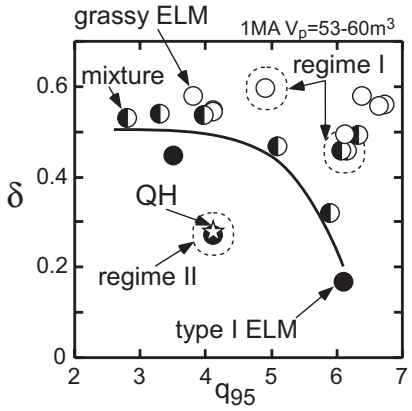

FIG. 1. q-δ operational space for grassy ELM and QH-mode. Dotted circles show target regions of the experiments for rotation effects in (I) grassy ELM regime and (II) QH-mode (type I ELM) regime, respectively.

radial extent of the collapse, normalized energy loss, and their comparison to the type I ELM. We also report that the effect of plasma rotation on the ELM characteristics in grassy ELM regime and QH-mode regime (well inside the type I ELM regime), as shown in Fig. 1, including discussions of the access condition to these modes.

2. Energy loss for grassy ELMs

The ELM energy loss for type I ELMs has been studied in many devises [7-10]. However, the ELM energy loss in the small ELM regimes such as grassy ELM and type II ELM regimes has not been well understood yet. Therefore, we report that how large amount of the plasma energy is released by grassy ELMs, and its comparison to type I ELMs. The plasma current of all plasma with the grassy ELM was 1.0 MA.

The improvement of the time resolution of the divertor D_α signal measurement in recent experiment make us possible to distinguish the signal of higher frequency ELM up to several kHz. Thanks to the improvement, we can classify grassy ELMs by high frequency periodic spikes in a divertor D_α signal. Figure 2 shows the comparison of ELM frequency (f_{ELM}) between grassy ELMs and type I ELMs, as a function of the power loss through the separatrix, P_{sep}. The frequency of grassy ELMs is about 15 times higher than that of type I ELMs, and the ELM frequency of both types increases with P_{sep}. For the type I ELM, the f_{ELM} can be considered as a consequence of the various timescales involved in the recovery of the pedestal energy to the pre-ELM level following the collapse. The similar relation between f_{ELM} and P_{sep} suggests that the f_{ELM} of the grassy ELM is also determined by the same mechanism. Therefore, the higher ELM frequency implies the smaller ELM energy loss (ΔW_{ELM}) in the grassy ELM. To confirm this hypothesis, the peak divertor heat flux of the grassy ELM was compared with that of the type I ELM as shown in Fig. 3. The peak heat flux at inner divertor target for grassy ELMs and type I ELMs were ~1.7 MW/m^2 and ~21 MW/m^2, respectively. The peak heat flux for the type I ELM was about 12 times higher than that for the grassy ELM, while the frequency of the grassy ELM was about 11 times higher. Therefore, the peak heat flux was almost in inverse proportional to f_{ELM}. The radial profile of the divertor heat flux for grassy ELMs seems to be smaller than that for type I ELMs. In order to conclude it, however, higher resolution of the heat flux measurement is required.

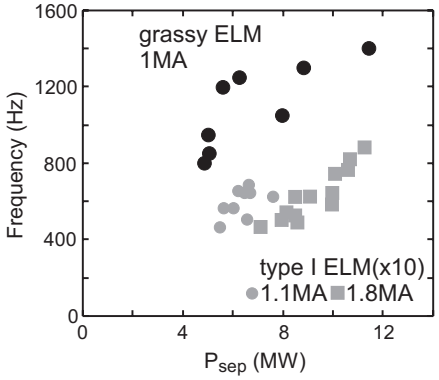

FIG. 2. ELM frequency as a function of P_{sep} ($P_{sep}=P_{abs}-P_{rad}-dW/dt$). Black symbols shows grassy ELM with δ~0.49-0.6 and q_{95}~4.1-6.7. Gray symbols are examples of type I ELM with δ~0.27 and q_{95}~3.1 and 5.1.

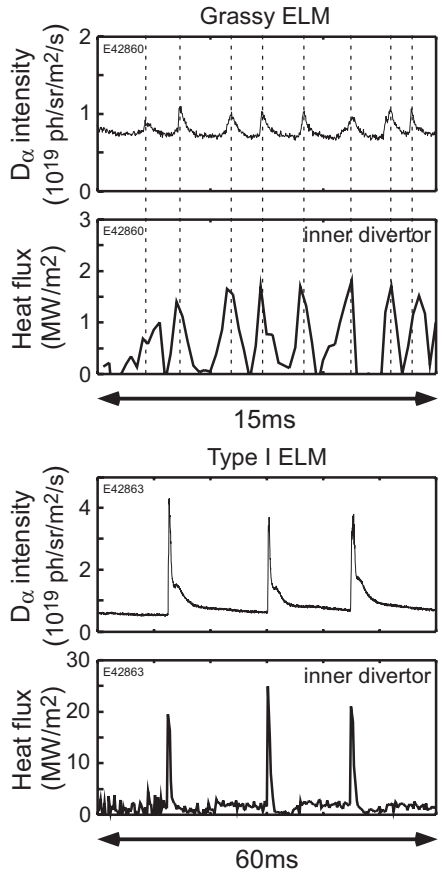

FIG. 3. Comparison of the divertor peak heat flux due to grassy ELMs (upper) and type I ELMs (lower). Frequency of grassy ELM was 533 Hz and that of type I ELM was 50 Hz.

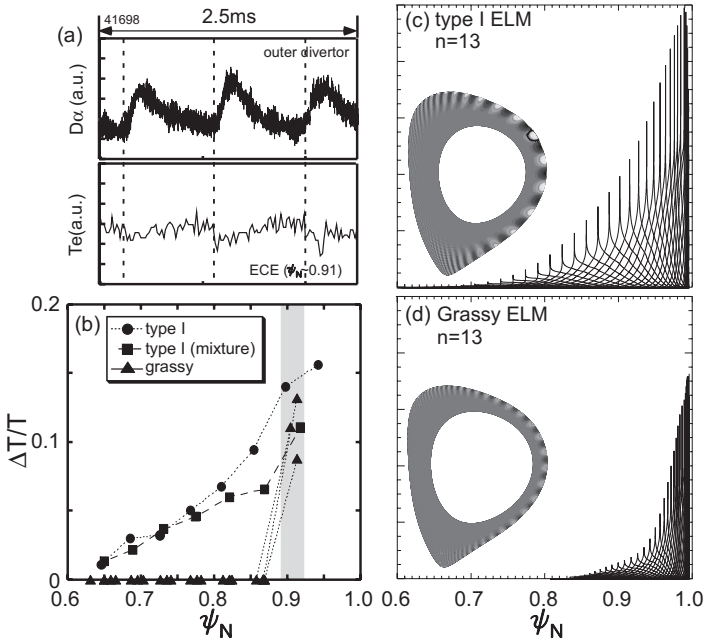

FIG. 4. (a) Time evolution of pedestal temperature. (b) radial profiles of normalized temperature reduction. Shaded region shows area of top of T_e pedestal. ELM frequency of type I ELM (closed circel) and type I ELM in mixture ELM phase (closed square) were 35 Hz and 40 Hz, respectively. (c) and (d) radial profiles and its poloidal distributions of eigen function of most unstable mode (n=13) for type I ELM (q_{95}~3.5) and grassy ELM (q_{95}~6.0), respectively.

In order to understand the reasons of smaller ELM size in grassy ELMs, we have studied the collapse of pedestal structure due to an individual ELM. In type I ELMy phase, a fast collapse of density and temperature pedestal has been studied by using a reflectometer and ECE radiometer, respectively [7, 11]. The reduction of pedestal temperature due to grassy ELMs was also observed in ECE signal as shown in Fig. 4(a). However, its radial extent was much narrower than that in type I ELMs as shown in Fig. 4(b), while the normalized temperature reduction at the top of pedestal approached a similar level. As for the collapse of density pedestal, a delayed and small reduction of the pedestal density as a result of the convective flow toward the collapse region near the low-field side midplane was observed by using the edge interferometer with the vertical chord at high-field side edge [12, 7], even when the collapse of pedestal structure is localized at low-field side. In the grassy ELM, on the other hand, clear reduction of pedestal density measured with the same interferometer as mentioned above has not been observed during pure grassy ELMy phase so far. One possible reason is that the amount of the density loss is quite small and the collapse is well localized in narrow poloidal region near the outer midplane. Figures 4(c) and (d) show the radial profiles of the eigen function of the approximately most unstable mode using ELITE code [13] as examples. Although a plasma parameter of q_{95}~3.5 for the stability analysis was different from that of q_{95}~6.2 for the experiment for the type I ELM case, a different radial distribution between type I ELM and grassy ELM is qualitatively consistent with the experimental results. These results may suggest that both type I ELM and grassy ELM is driven by the peeling-ballooning mode.

In JT-60U, the ΔW_{ELM} due to individual type I ELMs can be evaluated with good resolution by using the diamagnetic signal [7]. In the grassy ELM, on the other hand, no clear reduction of the diamagnetic signal enough to evaluate ΔW_{ELM} was observed so far. This result implies that the ΔW_{ELM} for the grassy ELMs is much smaller than that for type I ELMs. One possible way to evaluate ΔW_{ELM} is analyzing the change of the kinetic energy. As mentioned above, the density loss due to grassy ELMs seems to be small. Therefore, we can evaluate the conductive ELM energy loss, ΔW_{ELM}^{COND}, assuming $\Delta T_e=\Delta T_i$, spatially uniform Z_{eff} and including the dominant impurity of carbon, where

$$\Delta W_{ELM}^{cond} = \frac{3}{2}\int\left(1+\frac{7-Z_{eff}}{6}\right)n_e^{ped}\Delta T_e dV \qquad (1).$$

Since the poloidal asymmetry of the collapse of density pedestal has been observed in JT-60U [13, 7], it is considered that the collapse of temperature pedestal is also localized near outer midplane. However, the relaxation time scale of the electron temperature along the field line is much faster than convective one. Therefore, we can consider that the electron temperature has already become uniform in the same flux tube several μs after the collapse. Therefore, the observed reduction can be considered as a uniform value. Figure 5 shows the comparison of ΔW_{ELM} versus the pedestal stored energy, $W_{ped}=3/2\ (n_e^{ped}\ T_e^{ped} + n_i^{ped}\ T_i^{ped})\ V_p$, where n_e^{ped}, T_e^{ped}, n_i^{ped} and T_i^{ped} are the plasma parameters at the top of the pedestal, and V_p is the total plasma volume. The ΔW_{ELM} in the grassy ELM was 0.4-1% of W_{ped}, and this ratio is 10-20% of the ΔW_{ELM} in the type I ELM of 2-10% under various plasma conditions. Note that the ΔW_{ELM} in the type I ELM during the mixture ELM phase (open diamond in the figure), where the type I ELM and grassy ELM coexist in this phase, is smaller than that in the pure type I ELM phase. The different radial profile of the temperature reduction shown in Fig. 4(b) is one possible reason of the smaller ΔW_{ELM} in this mixture phase.

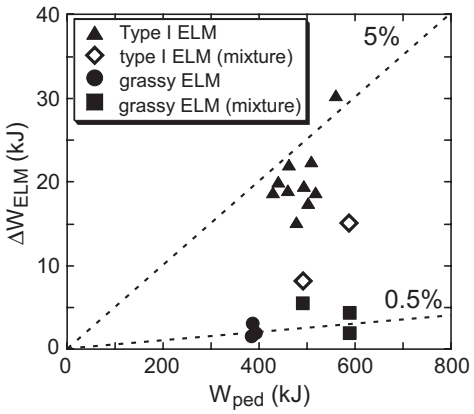

FIG. 5. ELM energy loss as a function of pedestal stored energy. ΔW_{ELM} for type I ELMs and grassy ELMs are evaluated by using diamagnetic signal and conductive energy loss from Eq. 1, respectively. The data for type I ELM shows same data of 1.1 MA plasma shown in Fig. 2 and 1.0 MA plasma shown in Fig. 3.

The ratio of the ELM loss power, P_{ELM} ($\equiv f_{ELM}\Delta W_{ELM}$), to P_{sep} for the type I ELM has often been considered as a constant value under the similar plasma condition such as similar plasma shape, edge density and temperature. The variation of this value for the plasmas with type I ELM shown in Fig. 5 was P_{ELM}/P_{sep} = 0.15-0.25. When the P_{sep} was varied in these plasmas, the f_{ELM} and ΔW_{ELM} were changed to maintain the ratio of P_{ELM}/P_{sep}. In grassy ELM, the similar relation was observed during power scan in one shot. When the heating power increased, the P_{sep} was increased from 5.0 MW to 8.0 MW. In this case, the f_{ELM} and ΔW_{ELM} were changed from 950 Hz to 1050 Hz and 1.7 kJ and 2.1 kJ, respectively. Then, the similar ratios of P_{ELM}/P_{sep} were observed, 0.31 in 5.0 MW phase and 0.27 in 8.0 MW phase, respectively. The variation of P_{ELM}/P_{sep} for grassy ELM was 0.27-0.47, which is twice higher than type I ELM case. Therefore, the larger amount of the power was carried by ELMs during the grassy ELM phase than type I ELM phase in spite of the narrower radial extent of the collapse due to the grassy ELM. Shorter inter ELM phase due to higher ELM frequency in the grassy ELM is one possible reason for higher P_{ELM}/P_{sep}.

3. Effects of plasma rotation on the ELM characteristics

3.1. Grassy ELM regime

The typical toroidal rotation profile in grassy ELM phase is shown by solid circle in Fig. 6(a), and Fig. 6(d) shows corresponding typical D_α signal. Although only CO NBIs among the tangential units were applied in this plasma, the edge plasma rotated in CTR direction as shown by solid circle in Fig. 6(a). The reason for this intrinsic CTR rotation has not been fully understood so far. It is considered that the ripple-induced fast ion loss injected by the perpendicular (PERP) NBIs may form a negative E_r [14, 15]. Therefore, in order to reduce the CTR plasma rotation, we replaced the PERP-NBIs with negative-ion based NBI (N-NBI),

which injects the beam in CO direction. On the other hand, the replacement of one CO-NBI by one CTR-NBI enlarged the CTR rotation slightly. During these rotation scan with fixed plasma shape, the ELM type was clearly changed from the type I ELM to the grassy ELM with higher frequency up to 1500 Hz, as shown in Fig. 6. As CTR rotation was increased, ELM frequency gradually increased together with the reduction of the ELM amplitude. Interestingly, the difference in the ELM amplitude between type I ELMs and grassy ELMs became smaller in the medium CTR rotation case shown in Fig. 6(c). Similar responses to the toroidal rotation on the ELM characteristics were observed in both operational points in regime I in Fig. 1.

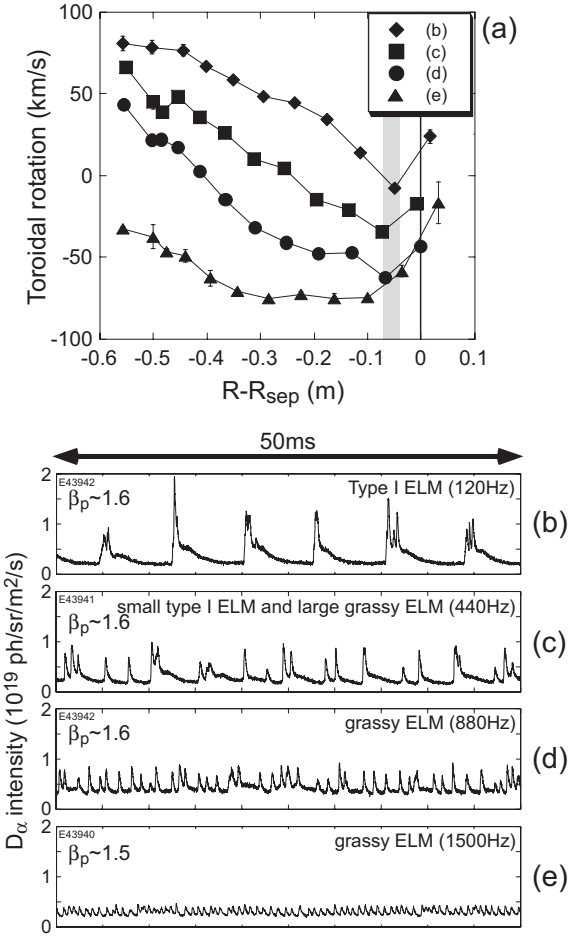

FIG. 6. (a) Toroidal rotation profiles mapped into outer midplane measured with charge-exchange recombination spectroscopy. Shaded region shows area of top of T_i pedestal. (b)-(e) Time evolution of D_α signal during plasma toroidal rotation scan at regime I in Fig. 1(q_{95}~4.9 and δ~0.59). Plasma rotation profiles were changed by using different combination of NBIs: (b) 2CO+2perp+2N-NB, (c) 2CO+3perp+1N-NB, (d) 2CO+5perp and (e) 1CO+1CTR+5perp.

These rotation scan was performed in a series of plasma discharges to keep the wall condition with fixed plasma configuration. The achieved poloidal beta, β_p, was also similar. It must be noted that pure grassy ELM was obtained at lowest value of β_p~1.5 as shown in Fig. 6(e). This result may suggest the larger counter rotation facilitates to access the grassy ELM phase. An interesting question is whether the absolute rotation magnitude or the rotation direction plays a more important role in the ELM physics. Since we cannot obtain larger CO rotation so far, farther experiments will require investigating this matter. It is also mentioned that the differences in the ELM frequency and size were very clear between Fig. 6(d) and (e), while the absolute value of the edge toroidal rotation was similar in these two case. Comparing the two rotation profiles carefully, a difference can be found in the structure of the rotation profile near the top of T_i pedestal. It is difficult to discuss this effect now, because the spatial resolution of the diagnostic is not enough. The dedicated measurement will be performed in the future experiments.

3.2. QH-mode regime (Type I ELM regime)

In the type I ELM regime with low δ, the change of plasma rotation affects the ELM frequency and amplitude, but the plasma usually remains type I ELMy phase. When the plasma position (clearance between the separatrix and the wall) was carefully optimized in regime II shown in Fig. 1, steady ELM free phase (QH-mode) with stationary pedestal parameters was obtained using two units of CTR NBI in 1.0 MA plasma as shown in Fig. 7. In this plasma, QH phase was kept constant for 3.4s, which corresponds to 18 τ_E, as shown in

Fig.7 (a) with the pedestal density of n_e^{ped}/n_{GW} ~0.28, where n_{GW} is the Greenwald density limit. The duration of the QH phase was only limited by the heating system. After the ELMy phase, the D_α signal remained at higher level together with the occurrence of the coherent temperature fluctuations (T_e fluctuation) with the frequency of ~9 kHz and ~18 kHz as shown in Figs. 7(e) and (f). On the other hand, no clear magnetic fluctuations with same frequency as T_e fluctuations were observed so far, may be due to the large distance from the separatrix and magnetic probe, and narrow radial distribution of the mode as discussed in the following.

Although the pedestal parameters during the QH phase were almost constant as shown in Fig. 7, their values in the QH phase were smaller than that in the ELMy phase as shown in Fig. 8, where the type I ELMs in this figure were obtained in the continuous series of the experiment with the same plasma configuration. Since there are many operational points of ELMy H-mode plasmas in similar pressure region for the QH-mode and confinement factor in QH-mode plasmas was $H_{89} \geq 1.5$, the plasma surely entered into the H-mode confinement regime.

Since the mechanism to reduce the edge pressure seems to be important to understand the appearance of the QH-mode, the radial profile of the edge T_e fluctuation was evaluated by scanning B_T slightly ~ 2% in one shot. As shown in Fig. 7(e)-(g), the fluctuation spectra responded to a change of B_T. During this phase, the T_e profile showing clear pedestal structure was obtained as shown in Fig. 9(a). The radial profile of the T_e fluctuation with the frequency of ~9 kHz were slightly narrower than the pedestal width, and the mode was localized at the edge ($R-R_{sep}$~2cm) as shown in Fig. 9(b). It is noted again that the pedestal parameters during this scan was almost constant as shown in Fig. 7. Therefore, we can consider that the mode structure and activity was constant during the scan for 1.6s (t=6.2-7.8s). A density fluctuation at outer midplane and a fluctuation in the ion-saturation current at the outer divertor target were also observed by using edge reflectometer and Langmuir probe. Figure 10 shows the comparison of these frequency spectra, and each signal was clearly modulated with the same

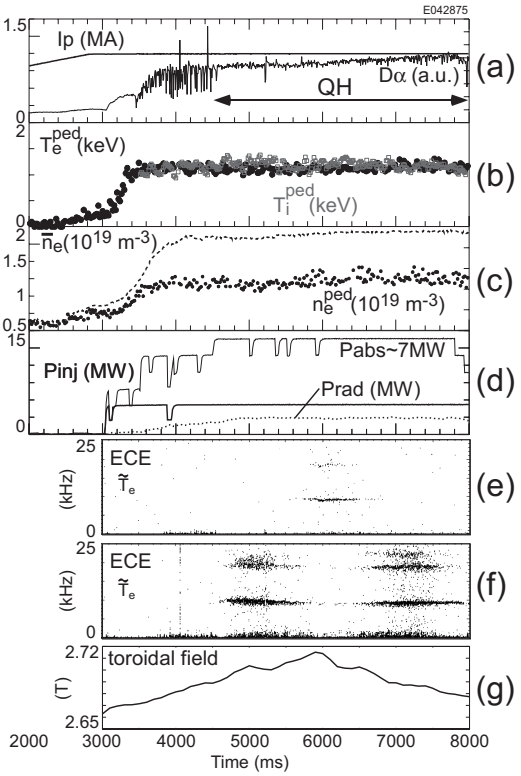

FIG. 7. Typical waveforms of QH-mode plasma in JT-60U. (a) plasma current and divertor D_α signal. (b) pedestal T_e (black) and T_i (gray). (c) line-averaged density and pedestal density. (d) Thin (thick) line show total (CTR) NBI power together with radiation power. (e) and (f) frequency spectrum in temperature fluctuation at f=119.5GHz and 118.5GHz channels, respectively. (g) Toroidal field strength.

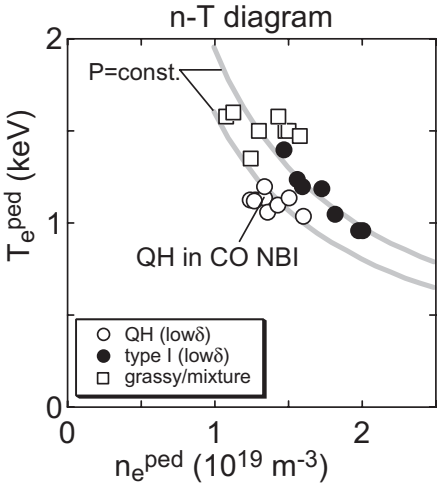

FIG. 8. Pedestal n-T diagram in QH-mode regime (regime II in Fig. 1) together with the grassy ELM regime (regime I in Fig. 1).

frequency. When the plasma rotation speed was changed, mode frequencies in all diagnostics were also changed, as shown in Fig. 11(b) and (c). These experimental results indicate that these coherent fluctuations in T_e and n_e play an important role to reduce the edge pressure. However, the relation between the appearance of edge fluctuations and the requirement of the optimized plasma position has not been understood yet.

In order to investigate the access condition to the QH-mode regime, the responses of the ELM and pedestal characteristics to the plasma rotation by changing the combination of tangential NBIs were investigated. Basically, CTR-NBI plasma seems to be easier to access

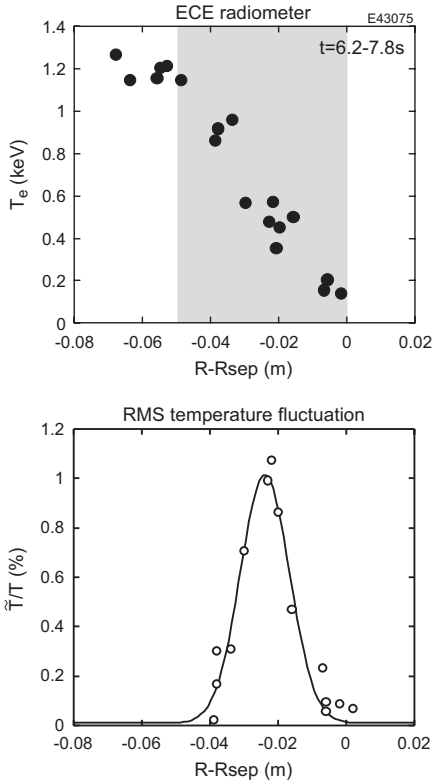

FIG. 9 (a) Temperature profile measured with ECE radiometer. Shaded region shows pedestal area. (b) Radial profile of T_e fluctuation for t=6.2-7.8s during B_T scan shown in Fig. 7(g).

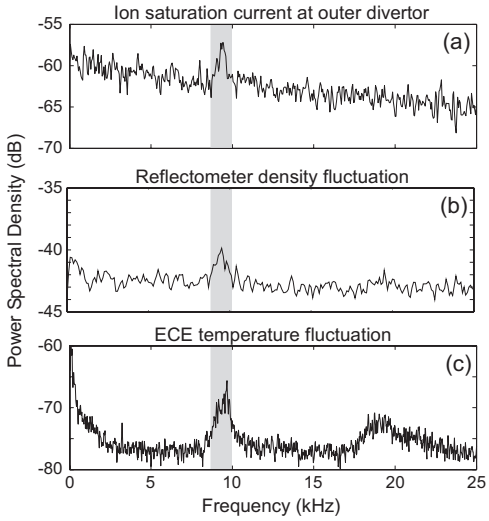

FIG. 10. Fluctuation spectrum in (a) ion saturation current (b) reflectometer with cutoff frequency of 34.1GHz (c) ECE radiometer.

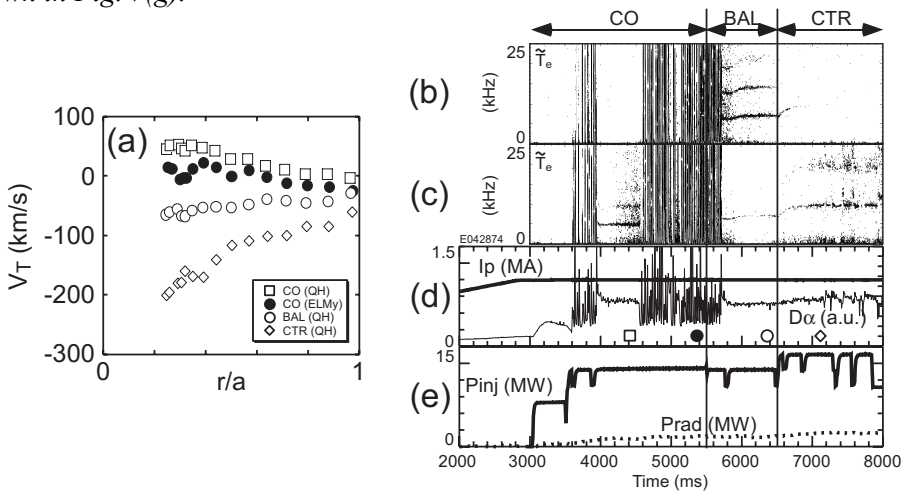

FIG. 11. (a) Toroidal rotation profiles during rotation scan. (b) and (c) frequency spectra of temperature fluctuations at f=119.5GHz and 118.5GHz channels, respectively. Changes in the spectra correspond to change of toroidal field same as Fig. 7(g). (d) plasma current and divertor D_α signal. Symbols in this figure show timing of rotation profiles in (a). (e) NBI power together with radiation power.

the QH-mode. However, we have also observed partial QH phase during CO- and balanced-(BAL-) NB injection. Figure 11 shows the results of rotation scan experiment in QH regime. As can be seen in Fig. 11(d), the behavior of divertor D_α signal to enter the QH-mode during CO-, BAL- and CTR-NB injection phase were mutually similar, and the occurrence of T_e fluctuation was also observed in all QH phases. The frequency of the mode varied with the toroidal rotation velocity as shown in Fig. 11(a)-(c). Similar to QH phase in CTR-NBIs, the onset of the mode reduced the edge pressure during the QH phase with CO-NBIs, as mentioned in Fig. 8. However, the increase of Z_{eff} was not so large compared with CTR-NBI phase as observed in P_{rad} shown in Fig. 11(e), and degradation of the confinement was also weak. In fact, the confinement factor at the QH phase during CO-NB injection phase at t=4.4s was H_{89}~1.7, which was comparable to that in the latter ELMy phase of H_{89}~1.8 at t=5.4s. It is noted that the edge rotation speed during QH phase under CO-NB injection phase was almost zero. Therefore, CTR-NB injections and a consequence of a CTR rotation may not be necessary conditions to access the QH-mode. Once we could understand how to control the appearance of these edge fluctuations, there is a possibility to expand the QH phase without CTR plasma rotation and CTR-NBIs.

4. Summary

The ELM energy loss of grassy ELMs was estimated to be 0.4-1% of the pedestal stored energy, which is smaller by factor of about 10 than that for type I ELMs of 2-10%. The reason of this smaller energy loss was characterized by narrower radial extent of the collapse of temperature pedestal. The different radial extent between type I ELMs and grassy ELMs qualitatively agrees with the different radial distribution of the eigen function of the approximately most unstable mode from the ideal MHD stability analysis. Then, this small energy loss leads to the higher ELM frequency. These ELM frequency and amplitude can be controlled by the toroidal rotation in the grassy ELM regime. The gradual change from type I ELM to high frequency grassy ELM was observed as CTR plasma rotation was increased. In QH-mode regime, on the other hand, the existence of edge fluctuations reduced the edge pressure due to the enhancement of the loss, as observed in higher base D_α signal and the modulated ion saturation current at the divertor target. Even in the CO-NB injection phase with no toroidal rotation, which is the similar operational condition in ITER, a transient QH-phase was observed simultaneous with the occurrence of the edge fluctuations.

Reference

[1] SHIMADA, M., Nucl. Fusion **44** (2004) 350.
[2] KAMADA, Y., Plasma Phys. Control. Fusion **42** (2000) A247.
[3] KAMADA, Y., Plasma Phys. Control. Fusion **44** (2002) A279.
[4] BURRELL, K.H., et al., Plasma Phys. Control. Fusion **44** (2002) A253.
[5] SAKAMOTO, Y., et al., Plasma Phys. Control. Fusion **46** (2004) A299.
[6] SUTTROP, W., et al., Plasma Phys. Control. Fusion **45** (2003) 1399.
[7] OYAMA, N., et al., Nucl. Fusion **44** (2004) 582.
[8] LOARTE, A., et al., Plasma Phys. Control. Fusion **44** (2002) 1815.
[9] LEONARD, A.W., et al., Plasma Phys. Control. Fusion **44** (2002) 945.
[10] URANO, H., et al., Plasma Phys. Control. Fusion **45** (2003) 1571.
[11] CHANKIN, A.V., et al., Nucl. Fusion **42** (2002) 733.
[12] OYAMA, N., et al., Nucl. Fusion **43** (2003) 1250.
[13] SNYDER, P.B., et al., Phys. Plasmas **9** (2002) 2037.
[14] KOIDE, Y., et al., Plasma Phys. Control. Nucl. Fusion Res. **1** 777 IAEA-CN-56/E-3-1.
[15] TOBITA, K., et al., Nucl. Fusion **35** (1995) 1585.